Supporting Information to:

Extended beta distributions open the access to fast gating in bilayer experiments: assigning the voltage-dependent gating to the selectivity filter

O. Rauh[1], U.P. Hansen[2], S. Mach[1], A.J.W. Hartel[3], K.L. Shepard[3], G. Thiel[1] and I. Schroeder[1§]

[1]Plant Membrane Biophysics, Technische Universität Darmstadt, Darmstadt, Germany
[2]Department of Structural Biology, Christian-Albrechts-University of Kiel, Kiel, Germany
[3]Department of Electrical Engineering, Columbia University, New York, NY, USA
[§]Corresponding author, Plant Membrane Biophysics, Technische Universität Darmstadt, Schnittspahnstraße 3, DE 64287 Darmstadt, schroeder@bio.tu-darmstadt.de

Supporting methods: High resolution experiments with a new type of bilayer array and amplifier

For the test of the reliability of the analysis by extended beta distributions, a new low-noise set-up was employed. A Meca-4 bilayer array with 50 µm apertures (Nanion Technologies GmbH, Munich, Germany) was connected to a VC100 low-noise, high bandwidth patch-clamp amplifier (Chimera Instruments, LLC, New York, NY, USA). Overload of the first stage was prevented by limiting the bandwidth to 20 kHz and enhancing it again by a subsequent boost filter up to 1 MHz. Signals were then passed through an antialiasing filter at 1 MHz and digitized at a fixed sampling frequency of 4 MHz. For the experiments here, they were filtered again using a digital 10-kHz 4-pole Bessel filter and sampled at 1 MHz. The resulting high noise related to the first 1 MHz filter leads to an increase of the quantization error of the 16-bit AD converter when it exceeds the signal. However, averaging by the subsequent 10-kHz filter reduces the "quantization noise" in the same way as the set-up noise (1, 2)

After channel incorporation, current measurements were performed at indicated membrane voltages. Measurements were done in the presence of 1 M KCl and 10 mM HEPES, pH 7.4, at room temperature.

Supplementary note 1: The improvements of the extended beta distribution fit over the classical beta distribution fit

The first application of beta distributions for fitting amplitude histograms of single-channel current (3, 4) opened the access to hidden fast gating events in ion channel research. It helped to overcome the problem that the inevitable baseline noise of the set-up requires a cut-off frequency of the low-pass filter, which often is too low for revealing the open-closed transitions of fast gating. Gating events with rate constants faster than the filter's cut-off frequency are smoothed out. Thus, the transitions can no longer be detected by level detectors. However, these transitions still lead to so-called excess noise (5, 6), which broadens the peaks in the amplitude histogram as compared to that one resulting from the baseline noise. A test with simulated data of how far this approach can look beyond the filter frequency was provided by Schroeder and Hansen (7).

The early investigations used an analytical expression for the calculation of the amplitude histogram resulting from hidden fast gating. However, this approach was restricted to Markov models with only two states (open and closed) and to low-pass filters of first order. However, in real

experiments, low-pass Bessel filters of 4^{th} or 8^{th} order are used and most ion channels have more than just two kinetic states. Yellen (4) employed an empiric correction factor to account for higher-order filters, which never worked in our investigations. Riessner (8) showed that the set of differential equations describing multi-state Markov model has no analytical solution and can be solved only by numerical methods. Even worse, also the constraints have to be implemented by an iterative procedure. Probably, these complications were the origin of the decay of the usage of beta distributions analysis after a blossom for some years.

In the meantime, the increase in computer power has enabled the calculation of theoretical amplitude histograms by simulated time series (6, 9, 10). The approach starts from a Markov model of gating like that one in Fig. 2A with an arbitrary set of rate constants and an assumption of the often unknown true open-channel current I_{true}. Two random number generators are employed. The first one determines the sink state with the relative probabilities weighted by the rate constants. The second random generator determines the point in time of the jump, again weighted by the rate constants. Since the dwell-times in some states can be much shorter than the sampling frequency, the time of the jumps is given in continuous time. At each jump, a step response of the actual low-pass filter is induced. The resulting time series is created from the sum of these step responses. This sum is calculated at the sampling points of the experiments. This provides a time series, which is sampled at the same times as the measured current trace. When adding the responses, the memory is limited. Preceding jumps are ignored when the sum of their responses has decayed below one bit. For the step responses, a theoretical response of the low-pass filter (as done in most cases) or a measured response can be used. We have verified that the response of our 4-pole Bessel filter exactly matches the measured one.

From the simulated, at this point still noise-free, time series, the amplitude histogram is generated. The baseline noise is introduced by a convolution of the amplitude histogram of the simulated time series with that one of the baseline noise. This can be a theoretical amplitude histogram (obtained from the width of the recorded baseline noise) or from a measured amplitude histogram. (In either case, sufficiently long sojourns in a closed state are required). The width of the baseline noise can also be readjusted during the fitting routine to give a good fit of the peak related to the closed state. That slope of the closed peak, which is on the side adverse to the open peak, is less distorted by transitions into the open state.

Of course, the amplitude histogram resulting from the first simulation run with a suggested set of parameters does not match the measured one. Then, the rate constants and I_{true} are readjusted in repetitive runs under the guidance of a simplex search algorithm (11) until a good fit of the theoretical amplitude histogram to the measured one is obtained.

Applying this method has enabled the study of ion/protein interaction and µs gating in BK channels (12, 13) or in viral Kcv channels (14) and the distinctions between the contributions of Ca^{2+} and of ion depletion to the negative slope conductance in BK at positive potentials (15). Even the analysis of a fast block with three conducting pores in OmpF became possible (16).

Supplementary note 2: Relationship between individual gating processes and characteristics of the amplitude histogram

As tested by simulated current recordings (17), the minimal number of states needed to fit an amplitude histogram (here, one open and three closed states, Fig. 2A) becomes obvious from the following characteristics in Fig. S1.

1.) In Fig. S1, the open peak is broader than the closed peak. This indicates a fast gating process, which starts from O with very short sojourns in a closed state called F (fast). In the current traces, this fast gating process causes a broadening of the apparent open level as compared to the closed level (Fig. S1A). In Fig. S1B, its influence has been removed by increasing k_{FO} and k_{OF} by a factor of 30, pushing them beyond the detection limit of the analysis.

2.) The slope between the open peak and the closed peak in Fig. S1 indicates a gating process slower than the O-F gating, but still beyond the cut-off frequency of the low-pass filter. This gating process (O–M "medium") causes the bursts and spikes seen in the current traces in Fig. 1C. Decreasing k_{OM} and k_{MO} individually by a factor of 2 indicates the strong correlation with the parallel shift and the steepness of the slope between the closed peak and the open peak, respectively, in Fig. S1C.

3.) State S (slow) accounts for the long sojourns in the closed state in Fig. 1C. The gating related to the O-S transitions determines the height of the valley between the closed peak and the open peak in Fig. S1 and the relative heights of these peaks. Decreasing k_{SO} and k_{OS} by a factor of 30 in Fig. S1B reveals its influence. Nevertheless, it is not recommended to evaluate slow gating by means of beta distributions as the analysis cannot distinguish between several slow gating processes. They have to be analyzed by dwell time distributions (18) or direct fit of the time series (19).

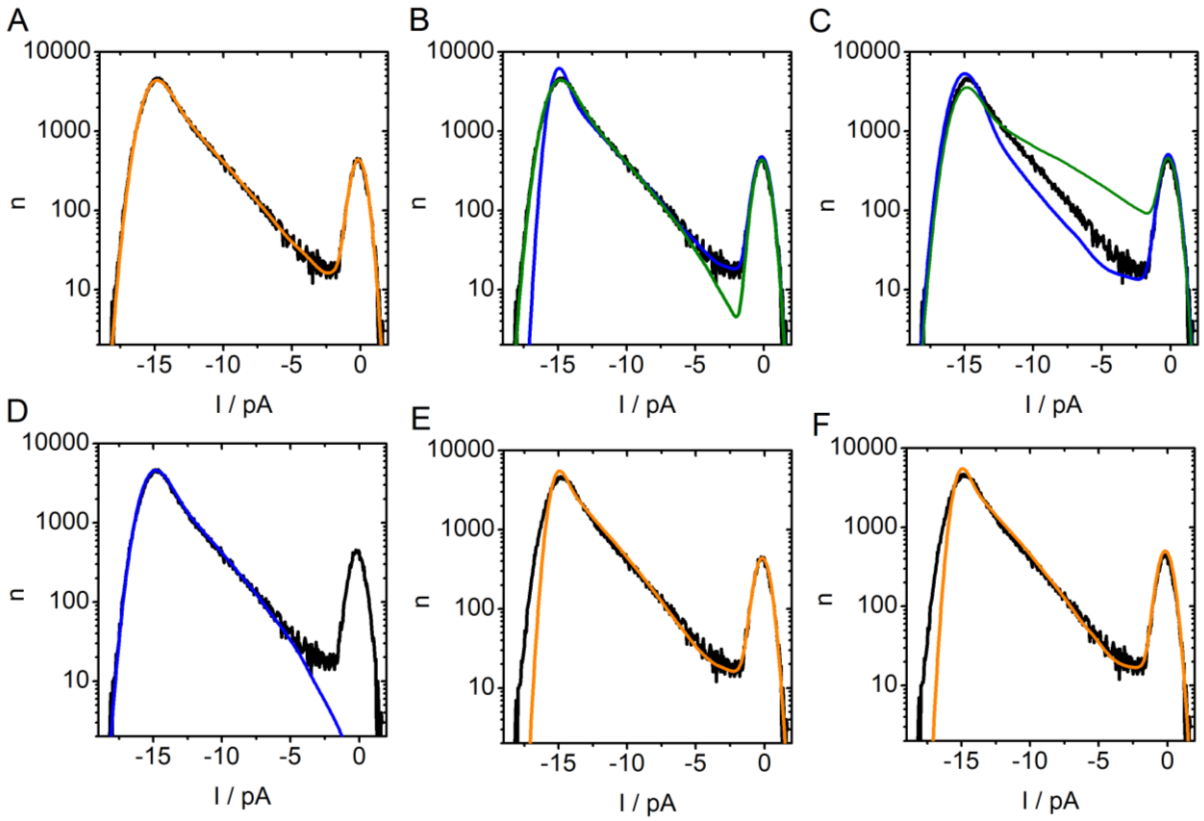

Fig. S1. Mutual independence of the influence of individual gating processes on an amplitude histogram (black) obtained from a current trace of Kcv_{NTS} measured in 1.5 M symmetrical KCl at -80 mV. **(A)** The orange line represents the best fit with the star-shaped model in Fig. 2A: I_{true} = 18.6 pA, k_{FO} = 373, k_{OF} = 92, k_{MO} = 17, k_{OM} = 1.9, k_{SO} = 0.236, k_{OS} = 0.014. All rate constants in ms^{-1}. **(B)** Influence of the O-S and O-F gating processes, demonstrated by changing parameters from the set in without subsequent fitting (A): Blue curve: O-F gating has been removed from the fit in (A) by multiplying k_{FO} and k_{OF} by a factor of 30, pushing them beyond the detection limit. Green curve: O-S gating has been removed by multiplying k_{OS} and k_{SO} by a factor of 0.03. **(C)** Influence of k_{OM} and k_{MO}: Blue curve: Parallel shift of the slope between the open and the closed peak by multiplying k_{OM} by a factor of 0.5. Green curve: decreasing the steepness of the slope by multiplying k_{MO} by a factor of 0.5 without subsequent fitting. **(D)** Eliminating state S of Fig. 2A. Amplitude histogram obtained with the rate constants of (A), but with k_{OS} and k_{SO} being omitted, without subsequent fit. **(E)** Result of a fit starting from the rate constants in (D), i.e. those of (A) with state S omitted. The results are I_{true} = 15 pA, k^*_{OS} =13.84, k^*_{SO} =273.8, k^*_{OM} =2174, k^*_{MO} = 20400. **(F)** Result of a fit starting from the rate constants in (A) with state F omitted. The results are I_{true} = 15 pA, k^*_{OS} =13.87, k^*_{SO} =273.6, k^*_{OM} =2137, k^*_{MO} = 20060. The lower value of I_{true} in (E) and (F) is caused by the exclusion of the F-O gating. All rate constants in s^{-1}. The asterisk means "rate constant numerically close to the corresponding one of the 3-state model".

Figures S1B and S1C illustrate that three closed states are required to model the amplitude histogram resulting from gating in Kcv and that the different gating modes are related to distinct regions of the amplitude histogram. Figures S1 D to F provide an alternative approach showing the necessity of three closed states in the model of Fig. 2A. This is done by reducing the number of closed states from three to two. In Fig. 1D, state S is taken out. This results in a complete absence of the C-peak. However, it could be argued that the remaining two gating mechanisms may take over the function of state S by an appropriate adjustment of their rate constants. Starting the fit from the rate constants of Fig. S1D leads to the fit in Fig. S1E. One of the two gating process takes care of the O-S gating in order to restore the C-peak. The remaining gating process is not capable of modeling both, the broadness of the O-

peak (resulting from O-F gating) and the slope between the C- and O-peak (resulting from O-M gating). Here, the fit algorithms takes the O-M gating more serious. In Fig. S1F, the F-state is omitted. The fit starts from the rate constants of Fig. S1A without k_{OF} and k_{FO}. The fit ends with up with rate constants nearly identical to those in Fig. S1E (legend of Fig. S1). Actually, this is not a surprise, because the computer does not know which state is omitted. There are two closed states, and during the fit routine they are defined in such a way that they give the best fit. The message is that three closed states are indispensable.

For the analysis here, the most important message from Fig. S1B,C is the low mutual interference between the different gating processes. Even strong misfits of the O-F gating or the O-S gating in Fig. S1B do not influence the slope between the closed peak and the open peak. Thus, they have a very small effect on the determination of k_{OM} and k_{MO}. This is the reason for the high reliability of the determination of k_{OM} and k_{MO}. Further details are given by refs. (Schroeder and Hansen, 2009a, b; Schroeder, 2015).

Supplementary note 3: Simplified equations for converting the topology of the Markov model from the branched one in Fig. 2A to the linear model S-O-F-M

Due to the large difference in the dwell-times in state F and M (Fig. 3B), it is not necessary to use the exact matrix transformations for the conversion of one model into another (20). In order to accurately describe the downward peaks of M-gating in Fig. 1C, the gross rate constants $g_{MO,L}$ and $g_{OM,L}$ of the linear S-O-F-M model must give the same number of transitions between O and M as $k_{MO,}$ and k_{OM} of the branched model in Fig. 2A. As shown in Fig. 3B, the dwell-times in F and M differ by a factor of 10. Under these numerical conditions, a reasonable estimate of the rate constants $k_{MO,B}$ and $k_{OM,B}$ of the O-M transitions in Fig. 2A (in the main text without index, but here represented by the index B for "branched") is given by the gross rate constants $g_{MO,L}$ and $g_{OM,L}$ in the S-O-F-M model (index L for "linear") (21).

$$k_{MO,B} \approx g_{MO,L} = \frac{k_{MF,L} \cdot k_{FO,L}}{k_{FO,L} + k_{FM,L}} \qquad k_{OM,B} \approx g_{OM,L} = \frac{k_{OF,L} \cdot k_{FM,L}}{k_{FO,L} + k_{FM,L}} \qquad \text{(S1a,b)}$$

Since the relatively few and slow transition between F and M in the linear model do not have a major influence on the transitions between O and F, we can assume that $k_{FO,L} \approx k_{FO,B} >> k_{FM,L}$. Thus, we can ignore $k_{FM,L}$ in the denominator of Eq. S1a and obtain

$$k_{MO,B} \approx g_{MO,L} \approx k_{MF,L} \qquad \text{(S2)}$$

Ignoring $k_{FM,L}$ in the denominator in Eq. S1b by the same argument leads to

$$k_{OM,B} \approx g_{OM,L} \approx k_{FM,L} \cdot \frac{k_{OF,L}}{k_{FO,L}} \qquad \text{(S3)}$$

$k_{FO,L}$ is about 10 times faster than $k_{OF,L}$ due to Figs. 3A and 3B (remember the O-F transitions have about equal rate constants in both models). Thus, $k_{FM,L}$ is faster than $k_{OM,B}$ in the branched model. This is necessary to produce the same number of transitions into the M state since the dwell time in F is very short. Since the ratio $\frac{k_{OF,L}}{k_{FO,L}} \approx \frac{k_{OF,B}}{k_{FO,B}}$ is quite constant (Fig. 3A,B, legend of Fig. S2), $k_{OM,L}$ and $k_{OM,B}$ differ by a nearly constant factor.

Supplementary note 4: Tests of the reliability of extended beta distribution fits

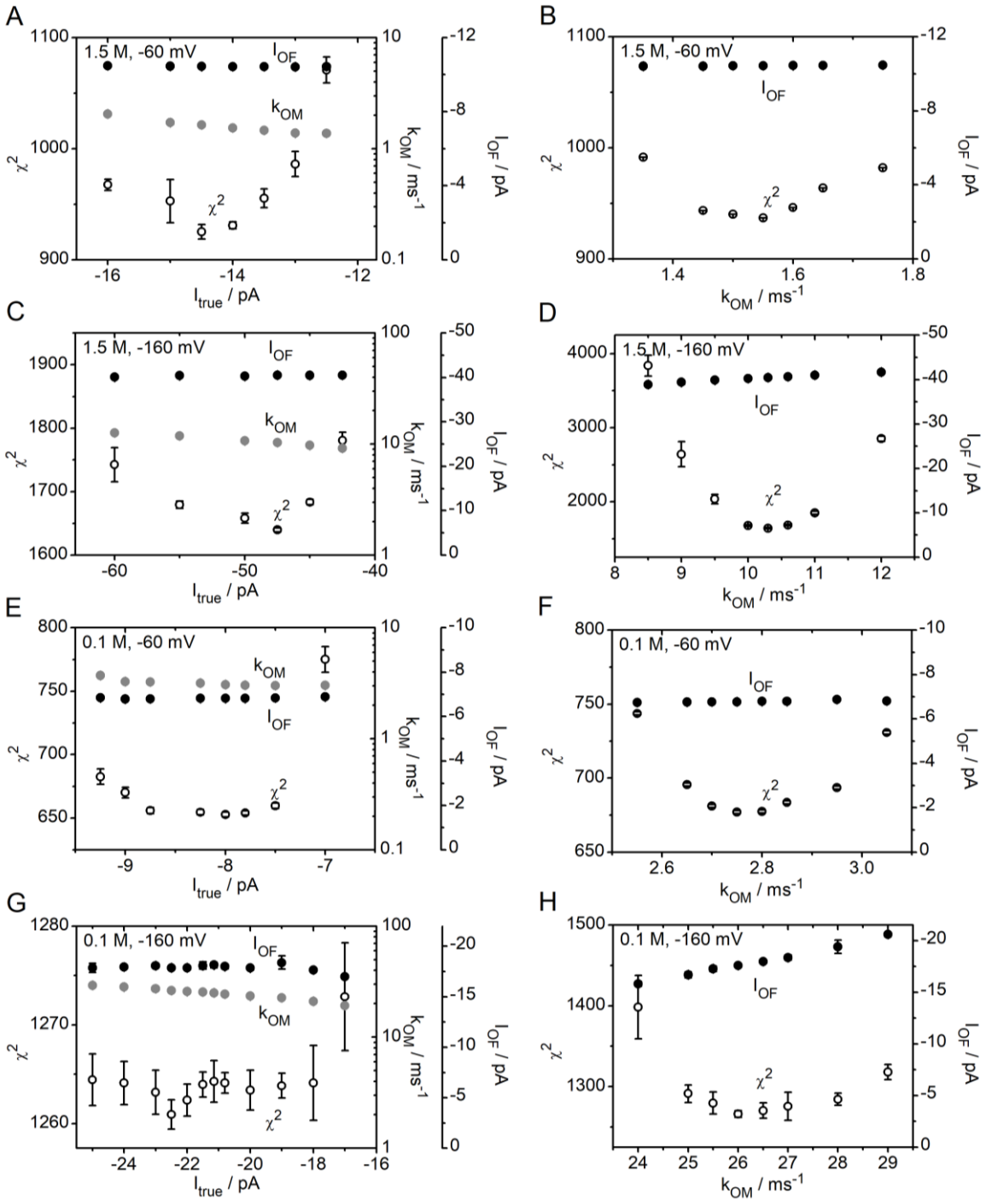

Fig. S2. Test of the reliability of the determination of current **(A,C,E,G)** and of the rate constant k_{OM} **(B,D,F,H)**. **(A,B)** Symmetrical KCl solution of 1.5 M at -60 mV with I_{OF}/I_{true} = 0.72 at the minimum. **(C,D)** Symmetrical KCl solution of 1.5 M at -160 mV with I_{OF}/I_{true} = 0.85**. (E,F)** Symmetrical KCl solution of 100 mM at -60 mV with I_{OF}/I_{true} = 0.85. **(G,H)** Symmetrical KCl solution of 0.1 M at -160 mV with I_{OF}/I_{true} = 0.79. The ratio I_{OF}/I_{true} has been determined at the minimum of the error. The values at the abscissa were set constant during the fitting routine and the other rate constants were free. The error plotted at the y-axis is $\chi^2 = \Sigma(\Delta n^2/n)$ with n being the number of sampling points per bin in the amplitude histogram. The standard deviations (if not hidden by the data points) results from 8 to 10 independent fits.

Figure S2 shows the dependence of the fitting error on the values of I_{true} and k_{OM} in symmetrical 0.1 M KCl and in 1.5 M KCl at -60 mV and -160 mV**.** At K^+ concentrations of 0.1 M, the open-channel current is smaller than that at 1.5 M. Consequently, the signal-to-noise ratio is decreased, and the minimum of the error sums becomes less pronounced. Nevertheless, the important finding is that the determination of I_{OF} (including averaging over the O-F gating, Eq. 1) is nearly independent of the choice of I_{true}, Especially, it is quite constant in the valley of the curve error versus k_{OM}. I_{OF} is about 80% of I_{true} (e.g., in Fig. 3A,B, legend of Fig. S2). Even though the minimum in Fig. S2G is weak it supports the finding in Fig. 3A,B and in the legend of Fig. S2 that k_{OF} and k_{FO} are quite voltage-insensitive.

Supplementary note 5: The relationship between the rate constant k_{OM} and k_{MO} and the gating factor *gf*

Equations 3 and 4 give an approximate phenomenological description of the voltage dependence of the two rate constants k_{OM} and k_{MO} of the O-M gating process. Inserting them into Eq. 5 for the gating factor *gf* (i.e. the "open probability" of the O-M process) leads to:

$$gf = \frac{k_{MO}}{k_{MO} + k_{OM}} = \frac{k_{MO,0} \exp(V / V_{MO})}{k_{MO,0} \exp(V / V_{MO}) + q_{OM} + b_{OM} \exp(-V / V_{OM})} \qquad (S4)$$

q_{OM} in the denominator has to be omitted because it is related to for a different mechanism at positive potentials (Fig. 6)

$$\begin{aligned} gf &\approx \frac{k_{MO,0} \exp(V / V_{MO})}{k_{MO,0} \exp(V / V_{MO}) + b_{OM} \exp(-V / V_{OM})} \\ &= \frac{\exp(V / V_{MO})}{1 + b_{OM} / k_{MO,0} \exp(-V \cdot (1 / V_{OM} + 1 / V_{MO}))} \end{aligned} \qquad (S5)$$

Eq. S5 is a Boltzman equation. However, gf_{min} is absent as compared to Eq. 5. Eq. 5 has been used for the phenomenological fit of *gf* in Fig. 5B. This implies that at high negative voltages, there is a deviation from the exponential form of k_{MO} (Eq. 4). There are some rare observations that the steepness decreases at negative voltages. A further investigation requires the usage of membranes, which tolerate higher negative voltages.

Supporting References

1. Rosenstein, J.K., S. Ramakrishnan, J. Roseman, and K.L. Shepard. 2013. Single ion channel recordings with CMOS-anchored lipid membranes. Nano Lett. 13: 2682–2686.
2. Hartel, A.J.W., P. Ong, I. Schroeder, M.H. Giese, S. Shekar, O.B. Clarke, A.R. Marks, W.A. Hendrickson, and K.L. Shepard. Ion channel recordings of the ryanodine receptor RyR1 at microsecond temporal resolution. under Revision
3. FitzHugh, R. 1983. Statistical properties of the asymmetric random telegraph signal, with applications to single-channel analysis. Math. Biosci. 89: 75–89.
4. Yellen, G. 1984. Ionic permeation and blockade in Ca^{2+}-activated K^+ channels of bovine chromaffin cells. J. Gen. Physiol. 84: 157–186.
5. Heinemann, S.H., and F.J. Sigworth. 1991. Open channel noise. VI. Analysis of amplitude histograms to determine rapid kinetic parameters. Biophys. J. 60: 577–587.
6. Schroeder, I. 2015. How to resolve microsecond current fluctuations in single ion channels: The power of beta distributions. Channels. 9: 262–280.
7. Schroeder, I., and U.-P. Hansen. 2009. Interference of shot noise of open-channel current with analysis of fast gating: patchers do not (yet) have to care. J. Membr. Biol. 229: 153–163.
8. Riessner, T. 1998. Level detection and extended beta distributions for the analysis of fast rate constants of Markov processes in sampled data. Aachen: Shaker Verlag.
9. Schroeder, I., P. Harlfinger, T. Huth, and U.-P. Hansen. 2005. A subsequent fit of time series and amplitude histogram of patch-clamp records reveals rate constants up to 1 per microsecond. J. Membr. Biol. 203: 83–99.
10. Schroeder, I., and U.-P. Hansen. 2006. Strengths and limits of Beta distributions as a means of reconstructing the true single-channel current in patch clamp time series with fast gating. J. Membr. Biol. 210: 199–212.
11. Caceci, M.S., and W.P. Cacheris. 1984. Fitting curves to data - The simplex algorithm is the answer. BYTE. 5: 340–362.
12. Schroeder, I., and U.-P. Hansen. 2007. Saturation and microsecond gating of current indicate depletion-induced instability of the MaxiK selectivity filter. J. Gen. Physiol. 130: 83–97.
13. Schroeder, I., and U.-P. Hansen. 2008. Tl^+-induced µs gating of current indicates instability of the MaxiK selectivity filter as caused by ion/pore interaction. J. Gen. Physiol. 131: 365–378.
14. Abenavoli, A., M.L. DiFrancesco, I. Schroeder, S. Epimashko, S. Gazzarrini, U.-P. Hansen, G. Thiel, and A. Moroni. 2009. Fast and slow gating are inherent properties of the pore module of the K+ channel Kcv. J. Gen. Physiol. 134: 219–229.
15. Schroeder, I., G. Thiel, and U.-P. Hansen. 2013. Ca^{2+} block and flickering both contribute to the negative slope of the IV curve in BK channels. J. Gen. Physiol. 141: 499–505.
16. Brauser, A., I. Schroeder, T. Gutsmann, C. Cosentino, A. Moroni, U. Hansen, and M. Winterhalter. 2012. Modulation of enrofloxacin binding in OmpF by Mg^{2+} as revealed by the analysis of fast flickering single-porin current. J. Gen. Physiol. 140: 69–82.
17. Schroeder, I., and U.-P. Hansen. 2009. Using a five-state model for fitting amplitude histograms from MaxiK channels: beta-distributions reveal more than expected. Eur. Biophys. J. 38: 1101–1114.
18. Blunck, R., U. Kirst, T. Riessner, and U.-P. Hansen. 1998. How powerful is the dwell-time analysis of multichannel records? J. Membr. Biol. 165: 19–35.
19. Albertsen, A., and U.-P. Hansen. 1994. Estimation of kinetic rate constants from multi-channel recordings by a direct fit of the time series. Biophys. J. 67: 1393–1403.
20. Kienker, P. 1989. Equivalence of aggregated Markov models of ion-channel gating. Proc. R. Soc. Lond. B. 236: 269–309.
21. Hansen, U.-P., O. Rauh, and I. Schroeder. 2016. A simple recipe for setting up the flux equations of cyclic and linear reaction schemes of ion transport with a high number of states: the arrow scheme. Channels. 10: 1–20.